Influence of Global Warming on Western North Pacific Tropical Cyclone Intensities during 2015

SE-HWAN YANG AND NAM-YOUNG KANG

National Typhoon Center/Korea Meteorological Administration, Jeju, South Korea

JAMES B. ELSNER

Department of Geography, Florida State University, Tallahassee, Florida

YOUNGSIN CHUN

National Typhoon Center/Korea Meteorological Administration, Jeju, South Korea

ABSTRACT

The climate of 2015 was characterized by a strong El Niño, global warmth, and record-setting tropical cyclone (TC) intensity for western North Pacific typhoons. In this study, the highest TC intensity in 32 years (1984–2015) is shown to be a consequence of above normal TC activity—following natural internal variation—and greater efficiency of intensity. The efficiency of intensity (EINT) is termed the "blasting" effect and refers to typhoon intensification at the expense of occurrence. Statistical models show that the EINT is mostly due to the anomalous warmth in the environment indicated by global mean sea surface temperature. In comparison, the EINT due to El Niño is negligible. This implies that the record-setting intensity of 2015 might not have occurred without environmental warming and suggests that a year with even greater TC intensity is possible in the near future when above normal activity coincides with another record EINT due to continued multidecadal warming.

1. Introduction

Tropical cyclones (TCs) in the western North Pacific (WNP), accounting for about one-third of all TCs in the world (Chan 2005), cause serious socioeconomic destruction over the Asia–Pacific region (Park et al. 2011; Peduzzi et al. 2012). A number of studies have investigated the connection between climate change and TC climate (Emanuel 2005; Elsner et al. 2008), suggesting that the warming ocean stimulates intensification of TCs. While most previous studies are based on trend analysis, correlation analysis by Kang and Elsner (2015) also shows that a warm environment, as inferred from global mean sea surface temperature (GMSST), enhances TC intensity. Trend analysis is

practically the correlation analysis between the standardized variable and time, while this study uses GMSST instead of time, making it free from the time range issue. GMSST has increased over the past 100 years, although in a series of steps and pauses. Especially over relatively short periods such as 1984–2015, and in parts of the world's ocean basins such as the western tropical Pacific, SST changes can be a combination of anthropogenic and natural forcing responses and internal variability (Fig. 1). Subsequently, Kang and Elsner (2016) present a hypothesis to explain how typhoons may get more intense, though less frequent, as global warming proceeds in coming decades.

According to the U.S. Joint Typhoon Warning Center (JTWC; https://metoc.ndbc.noaa.gov/web/guest/jtwc/best_tracks), the mean intensity of the TCs in 2015 was among the highest over the last 32 years (1984–2015). Here we deal only with WNP TCs whose lifetime-maximum intensity (LMI) exceeds $17 \, \text{m s}^{-1}$. Nine of the 27 WNP TCs during 2015 developed into super typhoons whose LMIs are defined as exceeding $66 \, \text{m s}^{-1}$ ($130 \, \text{kt}$; $1 \, \text{knot} = 0.51 \, \text{m s}^{-1}$). Typhoon Soudelor
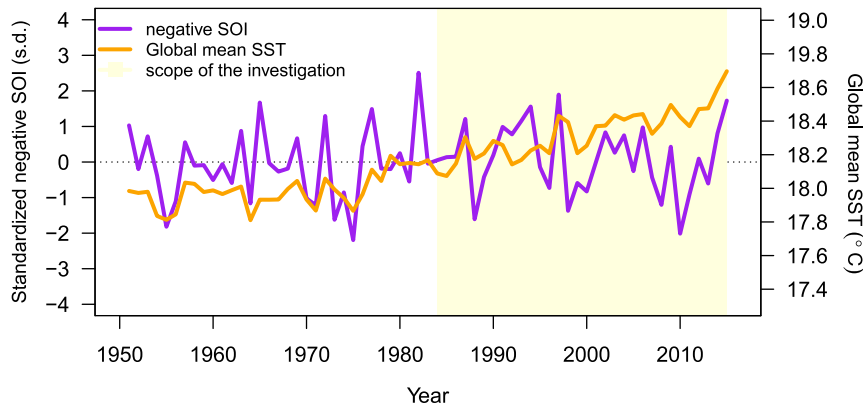
FIG. 1. Annual variation of the standardized values of global mean SST and negative SOI over the 65 years (1951–2015). JJASON observations are averaged and represented as annual values to represent the boreal summer environment for active TCs. Shaded period is the scope for this study.

reached a peak intensity of $79\,\mathrm{m\,s^{-1}}$, the strongest among the super typhoons in that year. It is well known that WNP TCs tend to be stronger during El Niño years (Camargo and Sobel 2005; Chan 2007) and 2015 was no different. But 2015 was also the warmest environment ever (Fig. 1), making it difficult to clearly identify the role each factor played in causing the intensity record.

In this paper we apply the theory of Kang and Elsner (2016) to help explain the record-setting 2015 WNP typhoon season. The application is a regression model that takes the El Niño–Southern Oscillation (ENSO) index and global sea surface temperatures as explanatory variables and returns prediction quantities for WNP TC intensity. From the perspective of the entire (1984–2015) record, El Niño represents primarily internal variability, while the GMSST changes are likely primarily a response to anthropogenic forcing and some natural forcings. Both El Niño and GMSST are correlated to variations in TC activity and intensity as depicted in Kang and Elsner (2016). The paper is organized as follows. Data are described in section 2. Indicators of WNP TC climate are explained in section 3. Contributions of the so-called blasting effect to 2015 intensity and the warming environment to the blasting effect are quantitatively examined in section 3 and 4, respectively. Results are summarized and discussed in section 5. Statistics and figures are made using the R programming language; the code is available at http://rpubs.com/namyoung/P2017.

2. Data

Best-track data from the Japan Meteorological Agency (JMA; http://www.jma.go.jp/jma/jma-eng/jma-center/rsmc-hp-pub-eg/besttrack.html) and from the JTWC are used for this investigation. Only TCs (LMI $\geq 17\,\mathrm{m\,s^{-1}}$) occurring

between June and November (JJASON) are included. The research period covers the 32 years from 1984 to 2015, inclusive. The range of years is selected to include as many observations as possible within the consensus period for the two best-track data sources (see Kang and Elsner 2012b).

The typhoon frequency and intensity data are modeled using the Southern Oscillation index (SOI) and GMSST as explanatory variables. Values for SOI come from the NOAA Climate Prediction Center (CPC; http://www.cpc.ncep.noaa.gov/data/indices/soi). Values for SST come from the Extended Reconstructed Sea Surface Temperature (ERSST), version 4 (Huang et al. 2016). For the investigation on the physical mechanism of the blasting effect during 2015, observed datasets are employed from monthly mean National Centers for Environmental Prediction (NCEP)–National Center for Atmospheric Research (NCAR) reanalysis data (Kalnay et al. 1996), such as geopotential height, air temperature, and specific humidity. Finally, all values each year are averaged over the months between June and November.

3. Merged indicators of WNP TC climate

Kang and Elsner (2012b) determined that two-dimensional TC climate formed by the indicators of frequency (FRQ), intensity (INT), activity (ACT), and efficiency of intensity (EINT). Kang and Elsner (2015) developed the framework into a three-dimensional variability space. For the better understanding, here we provide a brief explanation about the construction process of TC climate framework (see www.nature.com/article-assets/npg/nclimate/journal/v5/n7/extref/nclimate2646-s1.pdf). To investigate TC climate variability in this study, the framework is made by a
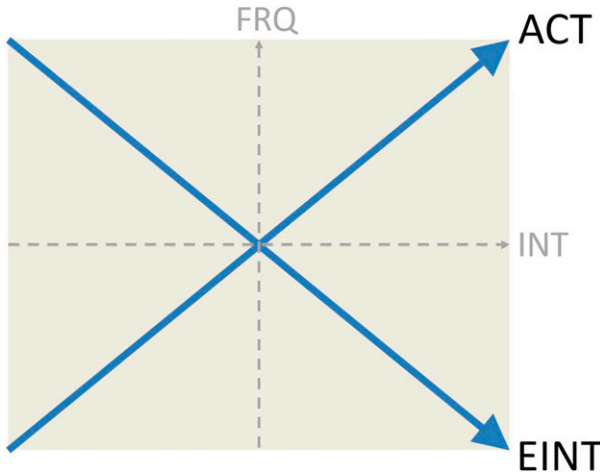
FIG. 2. The schematic of TC climate framework. The diagonal line labeled ACT indicates the in-phase relationship between FRQ and INT. The diagonal line labeled EINT indicates the out-of-phase relationship between FRQ and INT. Modified from Kang and Elsner (2012a).

principal component analysis (PCA) transformation of the FRQ and INT variables; that is, new directional variability space is constructed with these two variables FRQ and INT. INT is defined as the annual mean of only TCs intensities exceeding $17\,m\,s^{-1}$ and FRQ is the annual number of TCs above the threshold intensity of $17\,m\,s^{-1}$. A schematic diagram of the framework is shown in Fig. 2. A positive diagonal, denoted as ACT and the first mode of PCA between the FRQ and INT variables, indicates an in-phase relationship between the FRQ and INT variables, implying the variability in TC activity. This ACT value can be calculated as follows:

$$ACT = \left(\frac{INT - \mu_{INT}}{\sigma_{INT}} + \frac{FRQ - \mu_{FRQ}}{\sigma_{FRQ}} \right) \Big/ \sqrt{2}, \quad (1)$$

where INT and FRQ are annual values of intensity and frequency, and μ and σ indicate their respective mean and standard deviation. A negative diagonal, by contrast, indicates an out-of-phase relationship between the FRQ and INT variables, whose variability is denoted by EINT as the efficiency of intensity. In other words, EINT can explain what portion of INT is involved in ACT, and its additive inverse implies the efficiency of frequency. Likewise, EINT is simply calculated as

$$EINT = \left(\frac{INT - \mu_{INT}}{\sigma_{INT}} - \frac{FRQ - \mu_{FRQ}}{\sigma_{FRQ}} \right) \Big/ \sqrt{2}. \quad (2)$$

Kang and Elsner (2012b) presented a consensus between JTWC and JMA starting with 1984 when JMA employed Dvorak's satellite analysis technique (Dvorak

1975) to the operational typhoon intensity procedure (see www.wmo.int/pages/prog/www/tcp/documents/JMAoperationalTCanalysis.pdf). In this study, TC climates from the two independent agencies, JTWC and JMA, are merged to reduce the uncertainty associated with selecting a single source.

Values for each indicator are standardized for each best-track source, and then the principal component of the in-phase relationship is used for each merged indicator. Figure 3a shows the time series of ranked probabilities, representing the probability level from an empirical cumulative density of the annual values. The direction is plotted along the horizontal axis on the bottom, and I, A, F, and E denote INT, ACT, FRQ and EINT, respectively. These indicators are circularly linked with negative signs to make circular framework, and angles of 0°, 45°, 90°, 135°, 180°, 225°, 270°, 315°, and 360° denote I, A, F, −E, −I, −A, −F, E, and I, respectively. Figure 3b shows the difference between the two ranked probabilities (JTWC − JMA). The difference shows no systematic pattern, indicating that the two sources are providing essentially the same information. The relatively larger values between 2010 and 2015 around the EINT and INT directions confirm why JTWC observation suggests greater prominence in the trend of the derived EINT as examined in the previous study (Kang and Elsner 2016).

4. Contribution of EINT to the largest ever INT

According to Kang and Elsner (2012a) the annual variation in TC intensity can be understood as the linear combination of ACT and EINT. ACT, representing an in-phase relationship between INT and FRQ, indicates variability close to the well-known power dissipation index (PDI; Emanuel 2005) and accumulated cyclone energy (ACE; Bell et al. (2000) metrics. Annual values of PDI, ACE, and ACT in JJASON climatology over the 32 years show no increasing (or decreasing) trends (Table 1) (Klotzbach 2006; Kossin et al. 2007), although 2015 barely set a new record for annual mean LMI in the WNP.

Annual WNP TC intensity can be expressed by the addition of EINT and ACT as

$$INT_s = (ACT + EINT) \Big/ \sqrt{2}, \quad (3)$$

where the subscript s refers to a standardized value. Figure 4 shows the time series of WNP TC intensity. INT is shown as scaled by JTWC's mean and standard deviation. Orange (purple) shading indicates the positive (negative) contribution of EINT over ACT toward INT. Beginning with 1984 as a reference year for this study
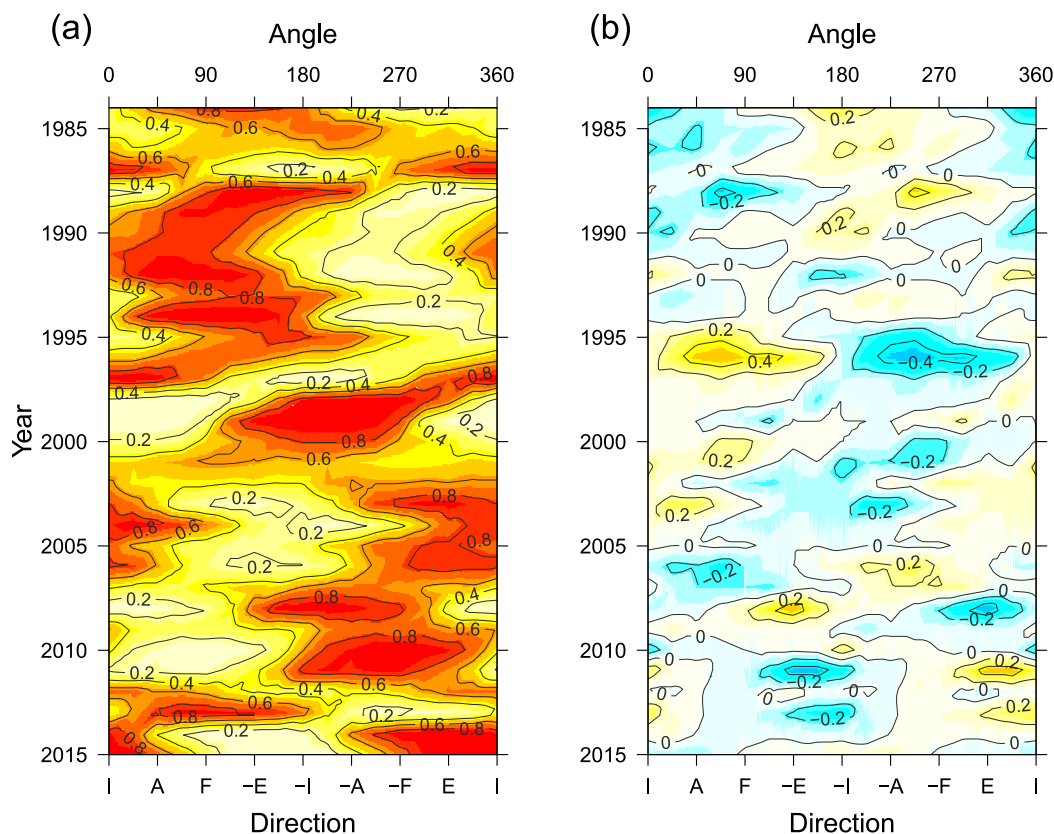
FIG. 3. Hovmöller diagram of (a) the annual variations of ranked probabilities in the merged WNP TC climate indicators during JJASON from JTWC and JMA best-track data (1984–2015), and (b) the difference between the ranked probabilities from the two observations. Probabilities are computed around the phase of the plane by the variable and principal component axes indicating INT, ACT, FRQ and EINT. INT, ACT, FRQ and EINT are denoted as I, A, F, and E. Angles of 0°, 45°, 90°, 135°, 180°, 225°, 270°, 315°, and 360° indicate I, A, F, −E, −I, −A, −F, E, and I, respectively. Contours denote the ranked probability, which represents the probability level from an empirical cumulative density of the annual values. Climate indicators (lower abscissa) and equivalent angles (upper abscissa) are shown along the horizontal axis. Modified from Kang and Elsner (2012b).

(dotted black line), EINT is seen to be increasing over time. The EINT contribution—an out-of-phase relationship between INT and FRQ by definition—implies that TCs "blast" more furiously (i.e., intensify more efficiently at the expense of TC occurrences). Clearly 2015 is the year of the strongest WNP TCs over the 32 years, and the EINT contribution is the largest ever. Compared to 1997 when El Niño previously affected the global climate (Bell et al. 1999), 2015 shows slightly stronger INT but with an apparently larger portion of EINT.

This study assumes that ACT is regulated by internal variation, in consideration of the regression slope having no trend (see Table 1). The green line in Fig. 4, representing the merged ACE (between JTWC and JMA), confirms again that this is ACT-like variation. Here, increasing intensity is interpreted as a consequence of adding EINT to the internal variation of

ACT. Probability levels of the occurrences of FRQ, INT, ACT, and EINT in 2015 are calculated as 0.31, 1.00, 0.72, and 0.97, respectively, among the 32 years. The strongest INT in 2015 is due to the contribution of both the above normal ACT and near highest level of EINT.

TABLE 1. Trend of WNP TC activity during JJASON over the 32 years (1984–2015). PDI, ACE, and ACT represent the merged variations from JTWC and JMA best-track data. P-val is computed under the null hypothesis of no trend. (Standard error is s.e.)

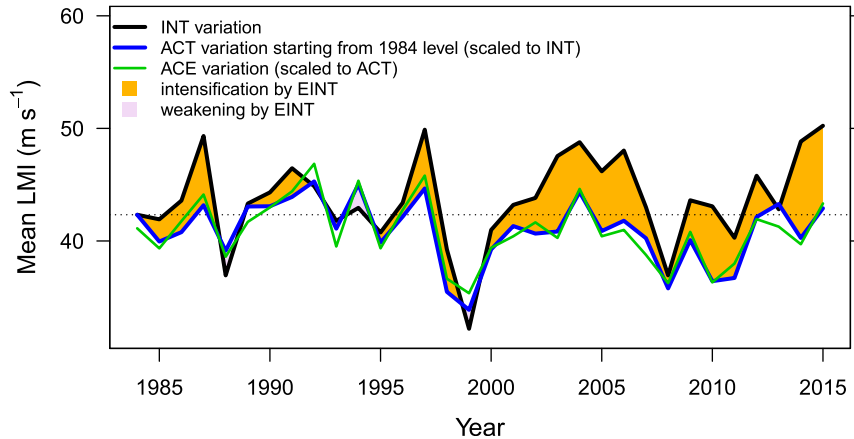| Statistic	Indicator		
	PDI	ACE	ACT
Trend (s.d. yr^{-1})	−0.02	−0.03	−0.03
s.e. (s.d. yr^{-1})	0.019	0.019	0.019
P-val	0.345	0.156	0.185

FIG. 4. WNP TC intensity (INT) compared to the portion of activity (ACT) during JJASON over the 32 years (1984–2015). The gap between INT and ACT is the portion of the efficiency of INT (EINT), which is the intensification at the expense of TC occurrences (blasting effect). ACT is also compared to accumulated cyclone energy (ACE), representing the similarity between the two metrics. TC activity indicated by ACT and ACE are seen to have no trend, while EINT shows an increasing trend.

5. Contribution of the warming environment to 2015 EINT

ACT in WNP TCs is tightly connected with ENSO variation indicated by the SOI, while EINT is significantly explained by the variation of global ocean warmth (Kang and Elsner 2015). A model for EINT can be fit using GMSST as

$$\text{EINT}_p = \alpha_1 \text{GMSST} + \beta_1. \tag{4}$$

An alternative model for EINT can be fit by adding the negative SOI (NSOI) variable, as

$$\text{EINT}_p = \alpha_2 \text{GMSST} + \alpha_3 \text{NSOI} + \beta_2. \tag{5}$$

Here EINT_p is the predictand of EINT; α_1, α_2, and α_3 are the regression coefficients for the explanatory variables, and β_1 and β_2 are intercepts. First, NSOI is used to indicate the variation of the ENSO warm phase (El Niño). SOI differs from ENSO indexes based on SST such as Niño-3, Niño-3.4, Niño-4, and so forth. The merit of using SOI is that the variation of the pressure difference between Tahiti and Darwin better reflects ENSO as an internal variation, since the SST warming trend is not directly involved. Correlation analysis between NSOI and time returns a value of −0.10 ([−0.43, 0.26], 95% CI), implying that the regression coefficient of standardized SOI by time is near zero.

Second, GMSST is used to indicate global ocean warmth. GMSST is a useful indicator of global warming in connection with TC climate change (Kang and Elsner 2015). Although these two environmental variables

show some physical coincidence by Bjerknes feedback (Bjerknes 1966), they are less coupled in the long term since GMSST has an internal variability and is also being forced to increase in sufficiently longer time scales, while NSOI is not. The correlation coefficient between these two environmental variables is +0.16 ([−0.20, 0.48], 95% CI).

From Eqs. (4) and (5), the departure of EINT from 1984 can be displayed. Figure 5 shows how much of the departure between modeled and observed (merged) EINT is explained by the synthetic environment of global warming indicated by GMSST and NSOI. The regression model by both GMSST and NSOI is not for prediction purpose but for quantitative examination of the ENSO contribution. GMSST explains 51% ($r = +0.71$; [.48, 0.85], 95% CI) of the observed EINT variation [see Eq. (4)], while the adjustment made by the ENSO contribution improves the explanatory power by only 2% [see Eq. (5)]. The magnitude of EINT during 2015, which is the major cause of record-breaking INT as seen in Fig. 4, is clearly due to this warming environment.

6. Summary and discussion

The year 2015 was characterized by El Niño and the warmest environment ever. Using a theoretical framework for the TC-climate structure developed by the authors in previous work, this paper clarifies the contribution of the warming environment to the record-breaking levels of WNP TC intensity. One can empirically decompose WNP TC metrics to reveal an offsetting influence of decreasing frequency and
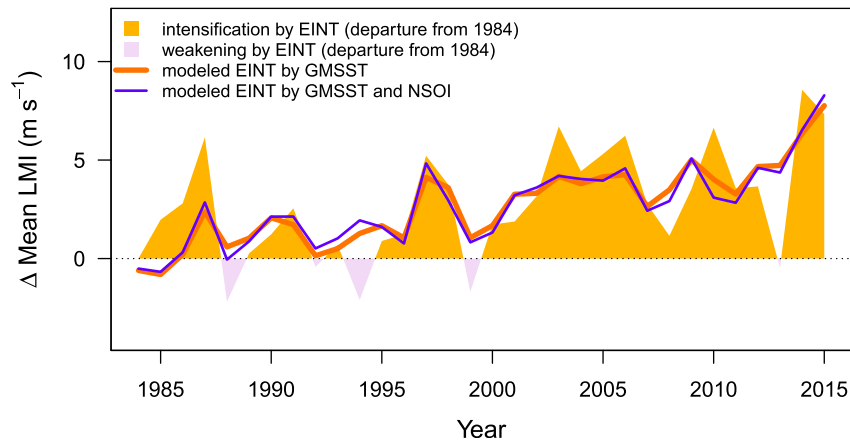
FIG. 5. EINT departure from 1984 and its modeled results. All values are averaged for JJASON and represented as INT scale. Regression model of EINT reveals that 2015 EINT is contributed mostly by the warming environment indicated by global mean sea surface temperature (GMSST). Additional contribution of El Niño environment indicated by the negative Southern Oscillation index (NSOI) seems negligible to the highest level of 2015 EINT.

increasing EINT, which are changes correlated to GMSST. By Kang and Elsner (2015), the GMSST contribution to EINT change was quantified from the climate change perspective. Current studies, on the other hand, quantify the contributions of global ocean warmth (indicated by GMSST) and ENSO (indicated by NSOI) to EINT on an annual basis. Quantities are given in LMI values, which enables direct comparison of annual ACT and EINT portions in INT amount. The modeling technique shown in this study is valued as a basis of operational climate prediction for typhoon intensity and frequency.

The annual variation (between 1984 and 2015) of the merged intensities for JJASON from JTWC and JMA are analyzed in this study. The out-of-phase relationship between the intensity and the frequency is seen to be increasing over time. We find that 2015 is the year of the strongest WNP TCs over the 32-yr period, and the EINT contribution is the largest ever. As EINT is defined, the result confirms that TCs ''blast'' more furiously at the expense of TC occurrences.

Regression models are fit to EINT using environmental factors as explanatory variables. The negative SOI and GMSST are used to indicate the two synthetic environments of El Niño and global warmth. Over relatively short periods, GMSST presumably depicts a combination of forced warming, episodic forced cooling from volcanoes, and internal climate variability. From a longer-term perspective, GMSST is assumed to be continuously increasing, which is still seen in the study period (see Fig. 1). The fitted model reveals that the 2015 EINT is mostly the result of the warming environment indicated by GMSST. The contribution of El

Niño is confirmed to be negligibly small in comparison. The results allow us to conclude that the record-breaking typhoon intensity of 2015 is the combined result of

- above normal ACT by internal variation, and
- very high levels of EINT statistically associated with high global SST values.

This conclusion implies that record 2015 INT might not have occurred without the environmental warming. It also implies that a year with an even stronger INT is possible when above normal ACT coincides with another record EINT associated with long-term global warming.

By providing probabilistic information based on El Niño and the state of global mean temperature, the regression approach introduced in this study has merit beyond the present work. The approach could help seasonal prediction modeling for WNP TC climate by outperforming the less skillful dynamic models that provide only deterministic values.

REFERENCES

Bell, G. D., M. S. Halpert, C. F. Ropelewski, V. E. Kousky, A. V. Douglas, R. C. Schnell, and M. E. Gelman, 1999: Climate assessment for 1998. *Bull. Amer. Meteor. Soc.*, **80** (5), S1–S48, https://doi.org/10.1175/1520-0477(1999)080<1040:CAF>2.0.CO;2.

——, and Coauthors, 2000: Climate assessment for 1999. *Bull. Amer. Meteor. Soc.*, **81** (6), S1–S50, https://doi.org/10.1175/1520-0477(2000)81[s1:CAF]2.0.CO;2.

Bjerknes, J., 1966: A possible response of the atmospheric Hadley circulation to equatorial anomalies of ocean temperature. *Tellus*, **18**, 820–829, https://doi.org/10.3402/tellusa.v18i4.9712.

Camargo, S. J., and A. H. Sobel, 2005: Western North Pacific tropical cyclone intensity and ENSO. *J. Climate*, **18**, 2996–3006, https://doi.org/10.1175/JCLI3457.1.

Chan, J. C. L., 2005: Interannual and interdecadal variations of tropical cyclone activity over the western North Pacific. *Meteor. Atmos. Phys.*, **89**, 143–152, https://doi.org/10.1007/s00703-005-0126-y.

——, 2007: Interannual variations of intense typhoon activity. *Tellus*, **59A**, 455–460, https://doi.org/10.1111/j.1600-0870.2007.00241.x.

Dvorak, V. F., 1975: Tropical cyclone intensity analysis and forecasting from satellite imagery. *Mon. Wea. Rev.*, **103**, 420–430, https://doi.org/10.1175/1520-0493(1975)103<0420:TCIAAF>2.0.CO;2.

Elsner, J. B., J. P. Kossin, and T. H. Jagger, 2008: The increasing intensity of the strongest tropical cyclones. *Nature*, **455**, 92–95, https://doi.org/10.1038/nature07234.

Emanuel, K. A., 2005: Increasing destructiveness of tropical cyclones over the past 30 years. *Nature*, **436**, 686–688, https://doi.org/10.1038/nature03906.

Huang, B., and Coauthors, 2016: Further exploring and quantifying uncertainties for Extended Reconstructed Sea Surface Temperature (ERSST) version 4 (v4). *J. Climate*, **29**, 3119–3142, https://doi.org/10.1175/JCLI-D-15-0430.1.

Kalnay, E., and Coauthors, 1996: The NCEP/NCAR 40-Year Reanalysis Project. *Bull. Amer. Meteor. Soc.*, **77**, 437–471, https://doi.org/10.1175/1520-0477(1996)077<0437:TNYRP>2.0.CO;2.

Kang, N.-Y., and J. B. Elsner, 2012a: An empirical framework for tropical cyclone climatology. *Climate Dyn.*, **39**, 669–680, https://doi.org/10.1007/s00382-011-1231-x.

——, and ——, 2012b: Consensus on climate trends in western North Pacific tropical cyclones. *J. Climate*, **25**, 7564–7573, https://doi.org/10.1175/JCLI-D-11-00735.1.

——, and ——, 2015: Trade-off between intensity and frequency of global tropical cyclones. *Nat. Climate Change*, **5**, 661–664, https://doi.org/10.1038/nclimate2646.

——, and ——, 2016: Climate mechanism for stronger typhoons in a warmer world. *J. Climate*, **29**, 1051–1057, https://doi.org/10.1175/JCLI-D-15-0585.1.

Klotzbach, P. J., 2006: Trends in global tropical cyclone activity over the past twenty years (1986–2005). *Geophys. Res. Lett.*, **33**, L10805, https://doi.org/10.1029/2006GL025881.

Kossin, J. P., K. R. Knapp, D. J. Vimont, R. J. Murnane, and B. A. Harper, 2007: A globally consistent reanalysis of hurricane variability and trends. *Geophys. Res. Lett.*, **34**, L04815, https://doi.org/10.1029/2006GL028836.

Park, D.-S. R., C.-H. Ho, J.-H. Kim, and H.-S. Kim, 2011: Strong landfall typhoons in Korea and Japan in a recent decade. *J. Geophys. Res.*, **116**, D07105, https://doi.org/10.1029/2010JD014801.

Peduzzi, P., B. Chatenoux, H. Dao, A. De Bono, C. Herold, J. Kossin, F. Mouton, and O. Nordbeck, 2012: Global trends in tropical cyclone risk. *Nat. Climate Change*, **2**, 289–294, https://doi.org/10.1038/nclimate1410.